A Mexican hat dance: clustering in Ricker-potential particle systems

D. Sabin-Miller*

University of Michigan, Center for the Study of Complex Systems

D. Abrams

Northwestern University, Engineering Sciences and Applied Mathematics

(Dated: November 5, 2024)

The dynamics and spontaneous organization of coupled particles is a classic problem in modeling and applied mathematics. Here we examine the behavior of particles coupled by the Ricker potential, exhibiting finite local repulsion transitioning to distal attraction, leading to an energy-minimizing "preferred distance". When compressed by a background potential well of varying severity, these particles exhibit intricate self-organization into "stacks" with varying sizes and positions. We examine bifurcations of these high-dimensional arrangements, yielding tantalizing glimpses into a rich dynamical zoo of behavior.

I. INTRODUCTION

Systems of coupled particles are a classic problem in physics and applied mathematics (e.g., [1–4] and many others). Here we investigate particles interacting via short-distance repulsion and long-distance attraction, often referred to as a "Mexican hat" potential (see Fig. 1). This qualitative scenario is seen in intermolecular forces and can be modeled via, e.g., the Lennard-Jones and Morse potentials.

Here we explore the behavior as one-dimensional populations of such particles are "squeezed" together, similar in concept to "particle in a box" considerations from quantum physics (e.g., [5]).

Local repulsion and distal attraction may call to mind the Lennard-Jones and Morse potentials from physics (see section A 2). These models for intermolecular potential energy have features rendering them distinct from our Ricker wavelet: infinite repulsion in the case of Lennard-Jones, and a "sharp" non-differentiable peak at the origin for Morse. However, these models may not be applicable in situations where coexistence at the same position is allowed, due to their nonphysical implications at $x = 0$. However, we believe a "smoothing" of the Morse potential's central peak (such as by integration against a "blurring" kernel function) would cause qualitatively similar results to what we observe in our Ricker system, and it is possible other "soft-core" potential systems (e.g., [6–8]) could find our results applicable. The smooth and coexistence-friendly dynamic embodied by our Ricker wavelet may also apply to neuronal phase models under proper conditions (e.g., [9–11]).

II. THE MODIFIED RICKER POTENTIAL

We use a modified form of the Ricker wavelet as the potential function carried or "worn" by each particle,

$$U(x) = \left[1 - \frac{k}{k-1}\left(\frac{x}{s}\right)^2\right] e^{-k\left(\frac{x}{s}\right)^2}, \tag{1}$$
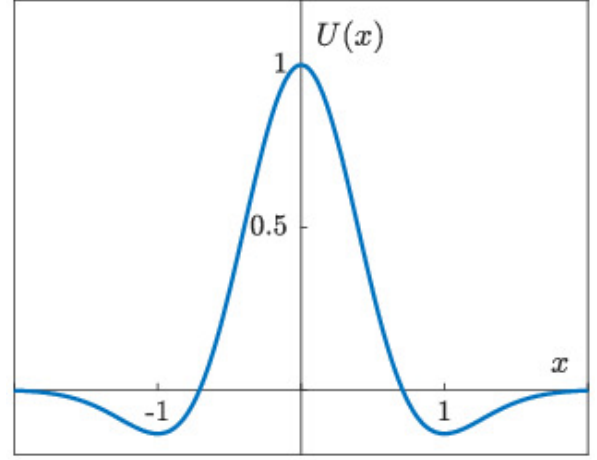
_____
* dasami@umich.edu

FIG. 1: **Ricker wavelet.** Interaction potential $U(x)$ for a particle described by the Ricker wavelet potential (Eq. (1)) with parameters $s = 1$ and $k = 2$.

which is pictured in Fig. 1.

This function has the following properties:

1. Central peak at $(0, 1)$

2. Symmetric troughs (i.e., local minima) at $x = \pm s$

3. Trough depth controlled by $k \in [1, \infty)$: as $k \to 1^+$, trough depth $\to -\infty$, and as $k \to \infty$, trough depth $\to 0^-$

Due to the central hump and symmetric troughs, this potential provides short-range, finite repulsion coupled with long-range attraction to a "preferred separation" s.

The potential at position x due to a particle at position x_i is

$$U(x|x_i) = \left[1 - \frac{k}{k-1}\left(\frac{x-x_i}{s}\right)^2\right] e^{-k\left(\frac{x-x_i}{s}\right)^2}. \tag{2}$$

We suppose that n particles, indexed 1 through n, have one-dimensional positions x_i and influence each other through their modified Ricker potential via the first order dynamical
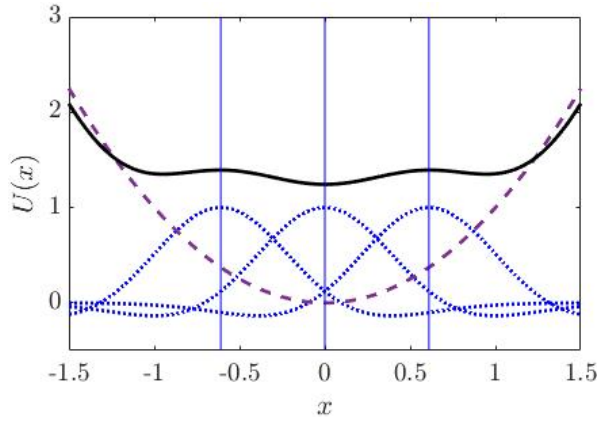
FIG. 2: **Three particles at equilibrium.** Example of three particles at an equilibrium. The vertical solid blue lines show particle positions, the dotted blue curves show the particles' potentials, and the dashed maroon parabola is the background potential well. The solid black curve is the total potential, and we can see the derivative is zero at each particle's position, indicating this arrangement is at equilibrium. This arrangement is stable: since a particle does not influences itself, each particle effectively "sees" the global potential minus its own contribution, which makes each particle's position in this arrangement a "trough" from its own point of view.

FIG. 3: **Equilibrium diagram.** Apparently stable equilibrium positions for 512 particles confined in a quadratic potential well. Color indicates particle abundance. The horizontal w-axis tick marks are placed at approximate bifurcation points, and persist on other diagrams of this type for comparison's sake. The horizontal scale is set by $w_0 = \frac{s}{k}\sqrt{\frac{k-1}{n}}$, which is the critical w value where the fully-stacked origin state becomes unstable (see section IV B). See section V for additional simulation details.

system

$$\frac{dx_i}{dt} = -\left.\frac{dU_{tot}}{dx}\right|_{x_i} = -\left.\left(\frac{dU_0(x)}{dx} + \sum_{j=1}^{n}\frac{dU(x|x_j)}{dx}\right)\right|_{x_i},$$

where confinement is imposed by the global potential function U_0, which we assume for simplicity to have a quadratic shape

$$U_0(x) = \frac{x^2}{w^2}$$

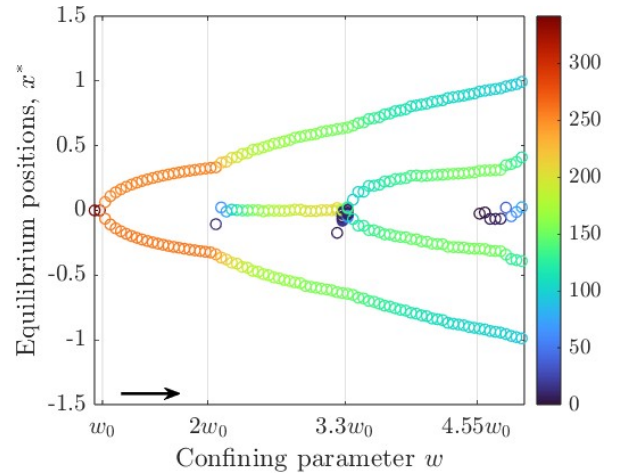with width-control parameter w. Figure 2 shows an example arrangement of particles in such a system.

We note for later reference the first and second derivatives of our Ricker potential:

$$\frac{dU}{dx} = -\frac{2k^2}{(k-1)s^2}x\left(1 - \frac{x^2}{s^2}\right)e^{-\frac{kx^2}{s^2}}, \quad (3)$$

$$\frac{d^2U}{dx^2} = -\frac{2k^2}{(k-1)s^2}\left[1 - \frac{3+2k}{s^2}x^2 + \frac{2k}{s^4}x^4\right]e^{-\frac{kx^2}{s^2}}. \quad (4)$$

In particular we note that due to the zero derivative of the Ricker potential at the origin, there is no need to complicate notation by explicitly excluding particles from influencing themselves; particles have no self-interaction regardless.

Without loss of generality, we henceforth restrict our analysis to the case $s = 1$, since an appropriate rescaling of space and time ($\tilde{x} = x/s$, $\tilde{w} = w/s$, $\tilde{t} = t/s$) removes that parameter

from the governing equations. The parameter k does qualitatively affect system behavior (which we briefly explore in Section (DSM: fix)S.2 of the Supplementary Materials (SM)), though our analysis is primarily concerned with the confinement parameter w. Unless otherwise noted, our numerical examples use the default parameter value $k = 2$.

A. Intriguing Collective Behavior

Free of confinement (i.e., with $w \to \infty$) and in the absence of any degenerate initial positions, particles will settle into a state of uniform spacing, with each particle residing at the preferred distance s from its neighbors. However, when confined, they exhibit highly nonuniform and rich behavior.

When confinement is present, we observe spontaneous organization of the particles depending on the choice of confinement parameter w (note that confinement is stronger as w decreases toward zero). Particles form "stacks"—states where multiple particles occupy the same spatial position—since their repulsion weakens as they get nearer to each other, but the number of particles in each stack can vary, and indeed the stacks exchange particles as w changes. We demonstrate this spontaneous organization in Fig. 3, which shows the results of numerical investigation of the system's stable equilibria.

Note that there is some slight asymmetry in Fig. 3 due to high dimensional multistability with various stack sizes; if we enforce symmetry, we see a picture of "core" behavior as shown in Fig. 4.
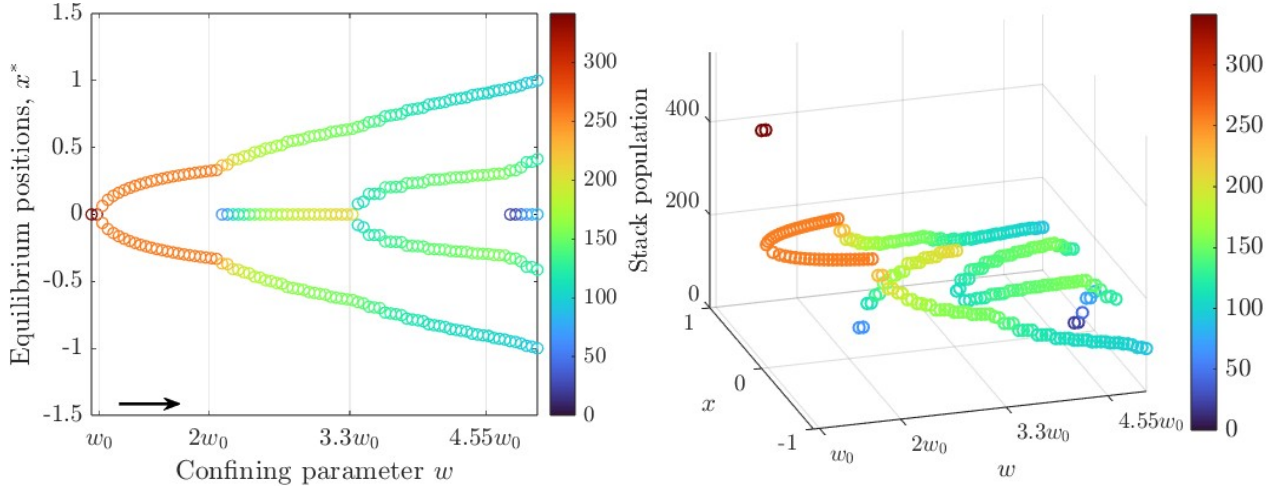
FIG. 4: **Equilibrium diagram,** $n = 512$**, symmetry enforced. Left:** A symmetry-enforced version of Fig. 3. Besides being "cleaner," however, we also notice the apparent bifurcation points change slightly due to the minimum of two particles in a stack. **Right:** A 3D view of the data in the left panel, with stack-size information encoded in the vertical axis as well as color. This emphasizes the continuous shift in population fractionation and the structure of the major bifurcations.
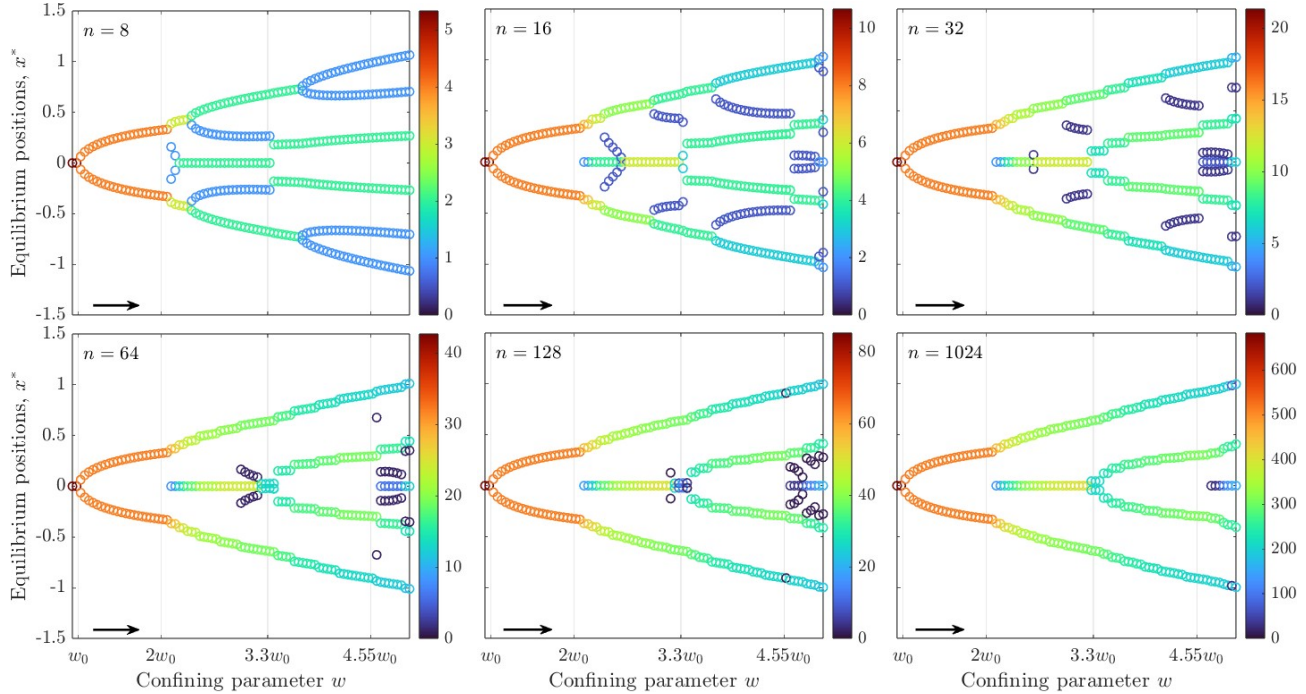

FIG. 5: **Symmetry-enforced system,** n **convergence.** Equilibrium diagrams for increasing population sizes n. The diagrams appear to converge in a visual sense to the same few "major" bifurcations, which occur at nearly the same multiples of the critical parameter value w_0 (given in Eq. (12)). This motivates us to understand and characterize this large-n generic behavior.

Also, note that these figures actually display 2-dimensional projections of an n-dimensional bifurcation diagram, with each particle's position occupying one dimension. However, the interchangeability symmetry of the particles allows the display of the whole population to serve as analogue for any single particle's possible positions.

The stack-size information (encoded by color) can be fur-

ther emphasized with a third dimension, as shown in the right panel of Fig. 4.

Thus we see even more clearly the pattern of stable behavior. For very small w (strong confinement, i.e., a narrow parabolic well) all the particles stack up at the origin, but the population splits apart into two symmetric stacks[12] when w passes a critical threshold we label w_0—we derive a formula

for this value (Eq. (12)) in the "Large n analysis" section. As w continues to grow, the stacks drift apart and the origin becomes stable again, and we see particles "fall" inwards to settle there. Initially only a few particles stably rest there, but as the stacks continue to separate the central stack grows, until it becomes large enough to split into two in a manner that appears similar to its initial bifurcation at $w = w_0$.

There are many other, more complex equilibria possible, but for large n the equilibrium diagram appears to become increasingly well characterized by the aforementioned behavior, as shown in Fig. 5. All the "major" bifurcations (birth of central stacks, splitting of central stacks) appear to happen at the same multiples of the critical parameter value w_0, thus with proper scaling of the w axis (to match w_0) the diagrams appear increasingly similar to one another.

We will start our exploration with smaller, more tractable examples and then progress from there to the more general, large-n cases.

III.   SMALL-n PARTICULAR CASE ANALYSIS

A.   Two-particle case

We can solve for the equilibrium condition on the right particle by assuming the particles are at $\pm x^*$ (plugging in $2x^*$ as the distance in equation (3) and adding the background potential at position x^*):

$$\frac{\mathrm{d}U_{\text{tot}}}{\mathrm{d}x}\bigg|_{x=x^*} = \frac{2x^*}{w^2} - \frac{4k^2 x^*}{(k-1)s^2}\left(1 - 4\frac{x^{*2}}{s^2}\right)e^{-\frac{4kx^{*2}}{s^2}} .$$

At equilibrium this slope is zero, thus $x^* = 0$ (corresponding to both particles stacked at the origin) or

$$0 = \frac{1}{w^2}e^{\frac{4kx^{*2}}{s^2}} - \frac{2k^2}{(k-1)s^2}\left(1 - 4\frac{x^{*2}}{s^2}\right) \tag{5}$$

So the bifurcation diagram (in w, k, or s) is given by the implicit equation (5). This corresponds to the exact solution

$$x^*(w) = \frac{1}{2}\sqrt{1 - \frac{1}{k}W\left(\frac{(k-1)e^k}{2kw^2}\right)} \tag{6}$$

$$x^*(w) = \frac{s}{2}\sqrt{1 - \frac{1}{k}W\left(\frac{1}{2}\frac{k-1}{k}\frac{s^2}{w^2}e^k\right)} \tag{7}$$

where W is the Lambert W function, defined as the solution to

$$W(z)e^{W(z)} = z . $$

Fig. 6 shows this solution overlaid on the empirical equilibrium diagram for two particles.

An approximation for $|x| \ll 0$ yields

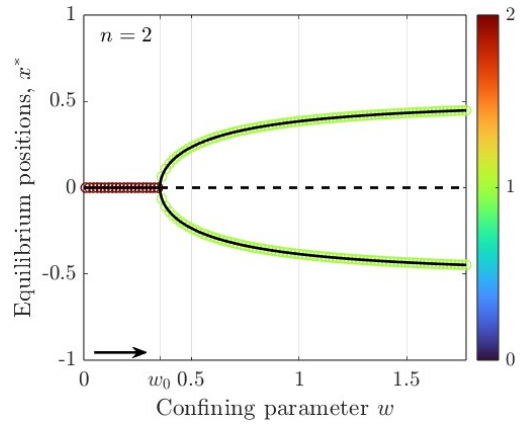$$x^*(w) \approx \frac{s}{\sqrt{2w_{0,2}(k+1)}}\sqrt{w - w_{0,2}} , \tag{8}$$

FIG. 6: **Two-particle bifurcation diagram, with exact solutions.** Equilibria for the two-particle system, with exact analytical solutions $x^* = 0$ (dashed when unstable) and Eq. (5) overlaid in black. The critical parameter value w_0 ($= \frac{1}{\sqrt{8}}$ in this case) is marked as well.

where we have defined $w_{0,2} = \frac{s}{k}\sqrt{\frac{k-1}{2}}$ as the lowest critical value of w with $n = 2$. We derive the general-n version (which we simply refer to as w_0 going forward) in the "Large-n analysis" section (Eq. (12)).

B.   Three- and four-particle cases

Three- and four-particle systems have unique stable equilibria for all w, which are shown in Fig. 7; unfortunately these resist such easy exact-solution form as the $n = 2$ case. Other equilibria exist for these systems (such as $1 - 2$ states[13] in the $n = 3$ case, $1 - 2 - 1$ and $1 - 3$ states in $n = 4$, and the fully-stacked origin state at $w > w_0$), but none of them are stable. In Fig. 8 we show all such equilibrium positions using the MatCont analytical-continuation software package for Matlab (MatCont v7.3, see [?]) to track those unstable artificially-partitioned states as well as the stable state we actually see in regular numerical simulations.
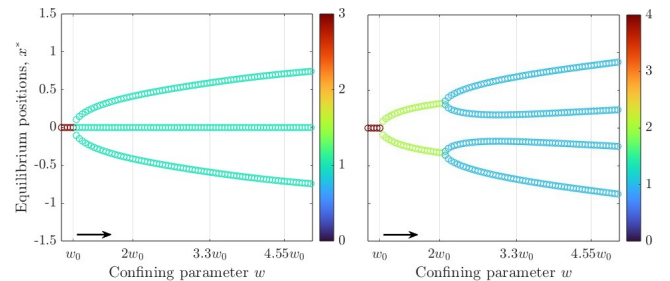

FIG. 7: **Three- and four-particle bifurcation diagrams.** Equilibria for 3-particle (**left**) and 4-particle (**right**) systems. For these small n, these are the only stable states. Note that we have shifted to using multiples of w_0 on the w axis, for comparison with higher n cases.

The nonzero stable branches for $n = 3$ (and $k = 2, s = 1$) are solutions to the implicit equation

$$e^{8x^{*2}} + (4x^{*2} - 4)w^2 e^{6x^{*2}} + (32x^{*2} - 8)w^2 = 0 ,$$

which is the result of assuming symmetry (one particle at 0 and the other two at x^*) and solving for nonzero x^* solutions to the equilibrium condition on the particle at x^*. For large $w \gg w_0$ this relationship converges to $w^2 = e^{2x^2}(4 - 4x^2)^{-1}$ (or explicitly in x: $x^2 = 1 - \frac{1}{2}W(\frac{1}{2}e^2/w^2)$); for w near w_0 ($w_0 = \sqrt{3}/6$) the relation is well approximated by $x^2 \approx 1/9 - 1/108\ w^{-2}$ instead.

In the 4-particle case, ($n = 4, k = 2, s = 1$) we can find the implicit equation for the $2 - 2$ (i.e. two stacks of two particles each) state, namely

$$w^2 = \frac{e^{8x^{*2}}}{16(1 - 4x^{*2})} ,$$

which is stable from $w = w_0$ ($= 1/4$ in this case) to $w \approx 2.1 w_0$ as seen in Fig. 7. More exactly, the $2 - 2$ state splits into the $1 - 1 - 1 - 1$ state when $w = w_c$, where

$$w_c^2 = \frac{1 + 20x^{*2} - 64x^{*4}}{16(1 - 4x^{*2})} ,$$

and where x^* satisfies the implicit equation

$$1 + 20x^{*2} - 64x^{*4} = e^{8x^{*2}} .$$

The $1 - 2 - 1$ state, while never stable, is also tractable, with outer stack positions given by the relation

$$8w^2 = \frac{e^{8x^2}}{1 - 4x^2 + (1 - x^2)e^{6x^2}} .$$

Other particular states may also have similar implicit equilibrium expressions, but their multitude makes this endeavor an impractical strategy for understanding the system for general n.

C. Five-particle system: birth of multistability

With five particles, we see the first case where there is multistability, by two different mechanisms. First of all, unlike $n = 3$ the origin cannot stably hold a particle as we cross w_0, and the population splits into a $3 - 2$ state, which is necessarily asymmetric in position. Then the indifference between which stack has 3 particles leads to bistability between two visibly different states, though they might be considered the same state up to reflection of the domain. Second, the point that the system drops to a $2 - 1 - 2$ state (on an increasing-w pass) is different from the point that it jumps back to the $3 - 2$ state (on a decreasing-w pass). We can see this in the difference between upper-left and upper-right panels in Fig. 9. This is because there is a region of bistability between $3 - 2$ and $2 - 1 - 2$ configurations—the loss of stability of $3 - 2$ happens at a higher w value than the gain of stability of $2 - 1 - 2$. This hysteresis with respect to increasing and decreasing parameter w is explored more generally in the "Medium-n analysis" section below.
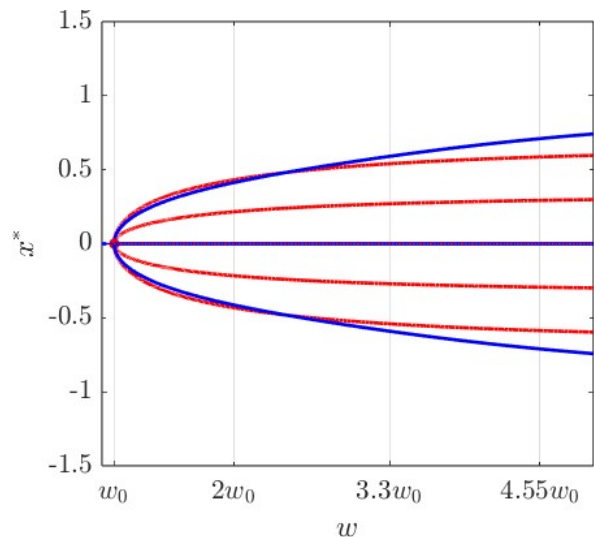

FIG. 8: $n = 3$ **bifurcation diagram, all equilibria.** The equilibrium diagram similar to the left panel of Fig. 7, but made with analytical-continuation software (MatCont v7.3)[?], showing unstable equilibria (in red) as well as stable ones (in blue). We note that since this is a 2D projection of a 4D bifurcation diagram (all three state variables are superimposed on the same vertical axis), stable and unstable branches appear to "cross" without exchanging stability but in fact belong to entirely different branches in state space. For example, the stable curved branches correspond to the outer particles of the $1 - 1 - 1$ state, while the red branches which cross them are for the single particle in the unstable $2 - 1$ state (meanwhile the inner branches correspond to the location of the 2-stack in that state). Similarly, the origin beyond w_0 is a stable position if the system is in the $1 - 1 - 1$ state but an unstable position for the fully-stacked state, so it is both blue and red-dotted in this figure.

D. Medium-n analysis

To get a sense of how the transition to the large-n behavior happens, we will look at a medium-scale n, in particular $n = 32$.

Figure 10 shows part of the bifurcation diagram for 32 particles, which shows hints of the dynamical process by which the particles transfer between stacks. At this resolution, we can see three "connecting" branches in the top right (decreasing-w) figure where single particle pairs transfer from the central stack to the outer ones.

Just as with the $n = 3$ and $n = 4$ diagrams, there are many more equilibria than we see in Fig. 10. First of all, we only see stable equilibria due to our method of forward-time numerical integration with minutely perturbed initial conditions, so we do not see the huge number of unstable equilibria. Second, we have enforced symmetry in this simulation, so we are missing the slightly asymmetric *stable* states that can (and generally do) result when particles are individually free; the enforcement of symmetry is nevertheless justified as we seek a generic central pattern around which many co-stable pertur-
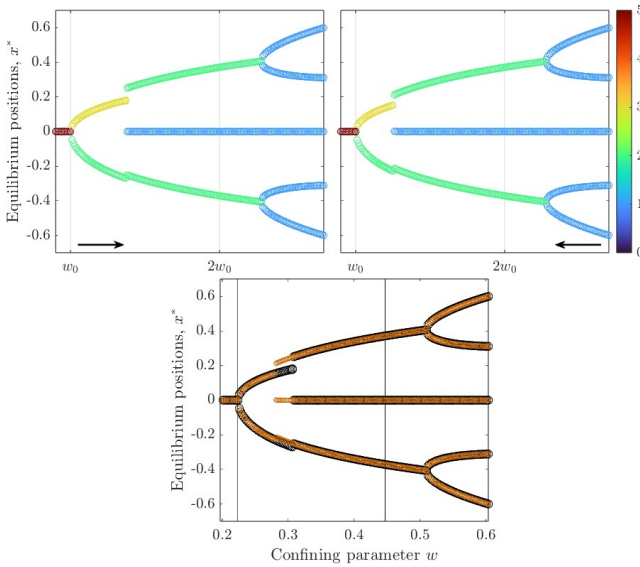
FIG. 9: **Increasing- and decreasing-*w* equilibrium diagrams, *n* = 5 particles.** Zoomed equilibrium diagrams for five particles. **Top Left:** increasing-*w* pass; note the asymmetric $3 - 2$ state arms are slightly longer. **Top Right:** decreasing-*w* pass, with shorter $3 - 2$ arms. The overlapping region exhibits bistability of $3 - 2$ and $2 - 1 - 2$ states.
Bottom: Overlay with increasing-*w* in black and decreasing-*w* in orange, emphasizing the area of bistability around $w = 0.3$. Previous w_0 multiple reference points persist as vertical lines, but decimal values are provided for finer reference.

FIG. 10: **Equilibrium Diagrams, *n* = 32, zoomed.** Bifurcation diagram for 32 particles, zoomed for higher resolution, displaying particle transfer branches and the system's multistability. **Top Left:** Increasing *w* pass, where particles "fall" to the center only when the outer stacks lose stability at their previous capacity. **Top Right:** Decreasing *w*, with particles transferring in three visible branches when the central stack becomes "overstuffed" and sheds particles to the outer stacks. **Bottom:** Both passes overlaid to emphasize differences, with forward pass in black and backward pass in orange.
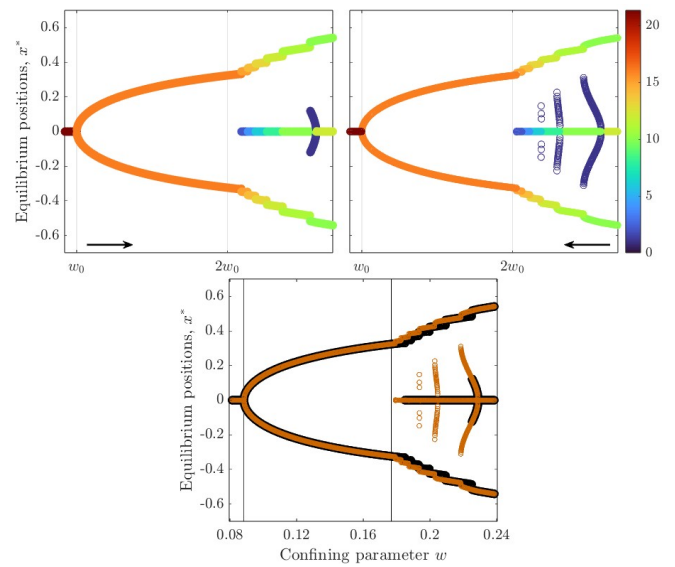
bations exist. But even in the symmetric case, there is co-stability of states, which is demonstrated by the discrepancy between increasing- and decreasing-*w* passes. Exploring these discrepancies will provide intuition about how the system behaves at higher *n*.

1. Repeated Hysteresis

The bottom panel of 10 emphasizes the differences between the increasing- and decreasing-*w* passes, with increasing-*w* pass in black and decreasing-*w* in orange. Two of those "branches" are isolated in Fig. 11.

To understand the hysteresis in Fig. 11, we start at the left side of the left-two figures, at $w = 0.2$. The top-left figure, a scatter plot of the full population, hides the stack-size information, but this is a $12 - 8 - 12$ arrangement in both black (increasing-*w*) and orange (decreasing-*w*) passes. The bottom-left figure shows us why; the "free" pair of particles may only stably exist at the outer stack positions for this parameter value (the central position is red, indicating instability).

As the parameter value increases, this arrangement stays stable until slightly under $w = 0.21$, when we see this branch undergoes a transcritical bifurcation. Theoretically, the pair could drift outward beyond the outer stack at this point, as the

lower-left figure indicates, but that diagram assumes the other stacks stay perfectly stacked, while in reality we perturb all particles with noise, and that state isn't robust to that broken symmetry. So what we actually see is that one pair falls to the origin and the rest remain together, corresponding to the $x^* = 0$ stable state in the bottom-left figure, and the overall population state $11 - 10 - 11$.

However, as we decrease *w* again, the system stays at this $11 - 10 - 11$ state until the branch point near $w = .205$, where the free pair's position follows stable branches away from the origin (in a $11 - 1 - 8 - 1 - 11$ state) until those branches go vertical in an apparent saddle-node bifurcation, at which point the pair jump suddenly to join the outer stacks again. During this bistable region, the position of the outer stacks differs slightly, which is reflected in the disalignment of outer stacks in the top-left figure.

A similar process occurs at slightly higher parameter value, reflected by the right two figures. In this case, the population is transitioning between $11 - 10 - 11$ and $10 - 12 - 10$ states. The only qualitative difference this time is the transcritical loss of stability at the outer position occurs *before* the central pitchfork bifurcation, so the outer pair is dropped to that branch of the pitchfork in a $10 - 1 - 10 - 1 - 10$ state on the forward pass rather than all the way to the center. On the backwards pass, of course, that $10 - 1 - 10 - 1 - 10$ state persists longer before losing stability and the transferring par-
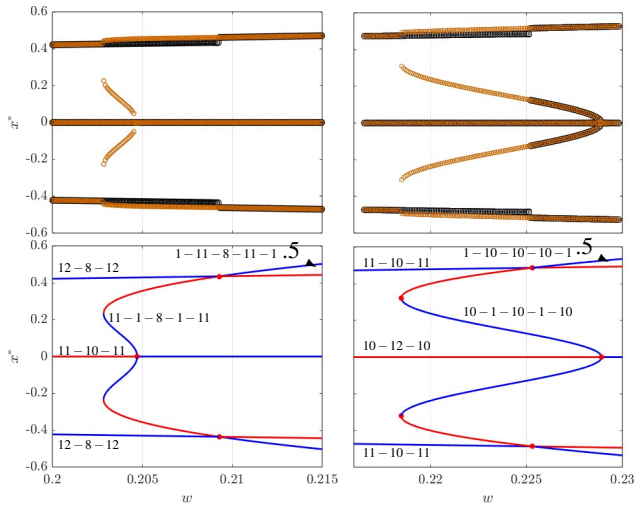
FIG. 11: **Particle-transfer branches.** Zoom views of central and right "transfer arms" from Fig. 10. **Top:** Overlaid scatter plots of the full-population equilibria, for forward (black) and backward (orange) passes. **Bottom:** Stability of states evaluated using MatCont analytical-continuation software, tracking locations where the transferring "free" particle pair can be—with stable positions are shown in blue, and unstable in red. The free pair may align with the other stacks (seen as effectively-horizontal lines, like the state labeled $12 - 8 - 12$; these persist through bifurcations but switch stability), or may reside in-between or outside them (e.g., the $11 - 1 - 8 - 1 - 11$ state which becomes $1 - 11 - 8 - 11 - 1$ in the bottom-left figure). The left figures explore the empirically observed transition from a $12 - 8 - 12$ state on the low w side to $11 - 10 - 11$ for higher w, and the right figures explore the transition from $11 - 10 - 11$ (lower w) to $10 - 12 - 10$ (higher w). For these parameters, $w_0 = 0.0884$.

ticles rejoin the outer stacks.

In this way, we see how bistability occurs between distinct population fractionations. As we can see in Fig. 10, the fractionation changes more rapidly when the central stack is small, which we may now understand causes these branches to overlap, yielding multi-stability between more than two fractionation states. Furthermore, as Fig. 5 displays, these transitionary states become narrower (in w) as n increases, such that we no longer easily see them at finite resolution. In the infinite-n limit, there is a continuous family of these bifurcations (and corresponding family of transition curves) as the central fractionation changes smoothly rather than in these discrete jumps, and smooth bands of stable fractionation (and corresponding stack positions) accordingly.

E. Large-n analysis

As Fig. 5 suggests, the overall system behavior appears to converge for large numbers of particles, under the appropriate scaling of the w axis. This makes discussion of the large-n limit meaningful—indeed it appears that the rapid "transi-
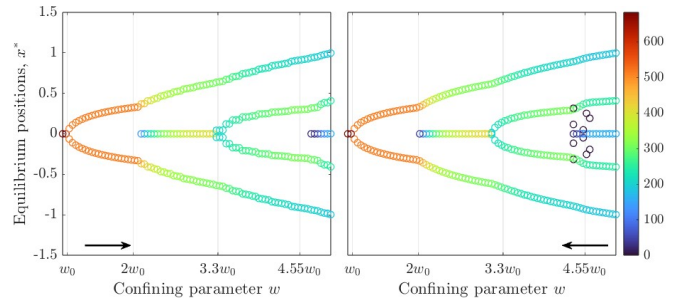

FIG. 12: **Equilibrium diagrams, large-n forward and backward passes.** Equilibrium diagrams for 1024 particles, with symmetry enforced. Some differences between forward and backward passes indicate the persistence of stability bands: we see different stable fractions of the population at the origin, and correspondingly different bifurcation points of the origin stack.

tionary" bifurcations from the previous section become effectively invisible, while the "major" central stack-birth/stack-splitting bifurcations remain. There is still fractionation indifference (i.e. bands of possible stable population percentages in each stack), and the location of these major bifurcations can still vary meaningfully between forward and backward parameter continuation, as Fig. 12 shows.

We can check the stability of particular configurations like we did in Fig. 8 for 3 particles, again using MatCont—for example, testing the stable and unstable equilibrium positions of a 129th "test" particle given 128 particles in two stacks of 64—this is shown in Fig. 13.

In Fig. 13 we see that the test particle can align with either of the large stacks (desymmetrizing their locations imperceptibly). But we also see that the birth of stability at the origin is in fact due to a second pitchfork bifurcation with very short-lived asymmetric unstable branches which cross the outer stack positions and become stable, roughly corresponding to sitting in the trough outside the two large stacks (and in fact approaching that well location, $\pm 3s/2$, as $w \to \infty$).

IV. ANALYSIS

A. General Equilibrium Statement

For particle j to be at equilibrium:

$$\frac{\mathrm{d}x_j}{\mathrm{d}t} = -\left.\frac{\mathrm{d}U}{\mathrm{d}x}\right|_{x_j} = 0,$$

$$0 = -\frac{2x_j}{w^2} + \sum_{i=1}^{n} \frac{2k^2(x_j - x_i)}{(k-1)s^2}\left(1 - \frac{(x_j - x_i)^2}{s^2}\right)e^{-k\frac{(x_j - x_i)^2}{s^2}}.$$

$$(9)$$

If the right hand side (RHS) is positive, particle j will move right, and if negative, left. If it is zero for all particles, the system is at equilibrium. There are many particular states,
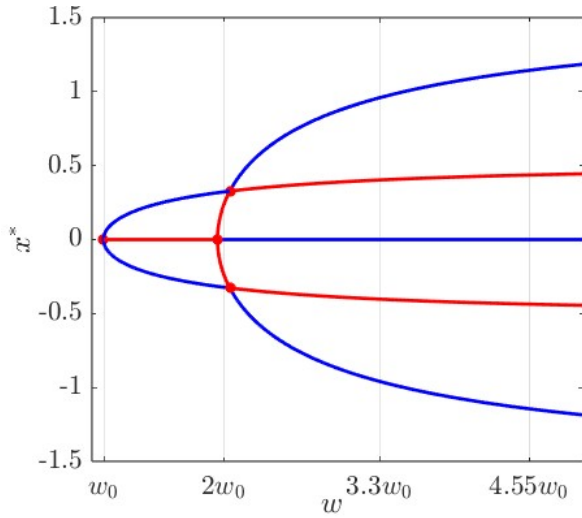
FIG. 13: **Stable and unstable equilibrium positions for a 129th particle.** Analytical-continuation software Matcont yields the stable (blue) and unstable (red) equilibrium positions for a 129th particle in a system with two perfectly-aligned stacks of 64 particles (which reside at the narrower U-shape, technically but imperceptibly influenced by the position of this 129th particle). We see that the "test particle" can stably align with those two stacks from $w = w_0$ up to slightly above $w = 2w_0$, the latter point occurring right after the birth of stability at the origin. At that point, it must either fall to the center or flee to the outside trough position.
In this context, we see stability at the center is born as a pitchfork bifurcation, and we may observe the small region of bistability shared between $64 - 65$ and $64 - 1 - 64$ states (which includes $2w_0$). For $n = 129$, $w_0 = 0.0442$.

such as all the particles at the origin $(0, 0, \ldots, 0)$, two symmetric stacks $(x^*, x^*, \ldots, x^*, -x^*, -x^*, \ldots, -x^*)$, etc., which may satisfy this equilibrium condition for various parameter values.

B. Stability

We can analytically examine the stability of the fully-stacked state at the origin, recovering the critical bifurcation value w_0 below which that state is stable—and in fact appears to be the *only* equilibrium.

The elements of the jth row of the Jacobian matrix J for the system (9) are

$$
\begin{cases}
J_{jj} = -\dfrac{2}{w^2} + \dfrac{2k^2}{(k-1)s^2} \cdot \\[2mm]
\quad \displaystyle\sum_{i=1}^{n} \left[1 - \dfrac{3+2k}{s^2}(x_j - x_i)^2 + \dfrac{2k}{s^4}(x_j - x_i)^4 \right] e^{-\frac{k(x_j - x_i)^2}{s^2}} \\[4mm]
J_{ji} = -\dfrac{2k^2}{(k-1)s^2} \cdot \\[2mm]
\quad \left[1 - \dfrac{3+2k}{s^2}(x_j - x_i)^2 + \dfrac{2k}{s^4}(x_j - x_i)^4 \right] e^{-\frac{k(x_j - x_i)^2}{s^2}}
\end{cases}
\tag{10}
$$

which, at the origin $x_i = x_j = 0$ (corresponding to the fully-stacked state), become

$$
J_{jj}|_O = -\frac{2}{w^2} + (n-1)\frac{2k^2}{(k-1)s^2} \; ,
$$

$$
J_{ji}|_O = -\frac{2k^2}{(k-1)s^2} \; .
$$

Due to the symmetry, we can identify all the eigenvectors:

1. The eigenvector $v_1 = (1, 1, \ldots, 1)$ corresponding to the full stack drifting left or right from the origin has eigenvalue $\lambda_1 = -2/w^2$, which is always negative, indicating that the 1-stack system is stable to these types of perturbations (unsurprising based on intuition for a single particle).

2. The other $n-1$ eigenvectors consist solely of symmetric two-particle divergence; i.e., vectors of the form $(-1, 1, 0, 0, \ldots, 0)$ with the positive 1 in each of the other $n-1$ positions. These vectors all have eigenvalue $\lambda = -2/w^2 + 2nk^2/(k-1)s^2$. The 1-stack state is thus stable to these types of perturbations for

$$
\frac{w}{s} < \frac{1}{k}\sqrt{\frac{k-1}{n}} \; .
\tag{11}
$$

Solving for w, this gives us the critical parameter value w_0 for general n:

$$
w_0 = \frac{s}{k}\sqrt{\frac{k-1}{n}} \; .
\tag{12}
$$

We note that this agrees with the $n = 2$ particular case, given above after Eq. (8). This also suggests the appropriate way to rescale the w axis as n varies (as we have for all figures), since the structure appears to depend only on the ratio w/w_0 (at least asymptotically for large n).

C. Two-stack state

The simplest nontrivial arbitrary-n case, the two-*stack* state—where the population is split into two symmetric stacks of $n/2$ particles each—is quite relevant to examine since it is

the dominant behavior for approximately $w_0 < w < 2w_0$. It is exactly solvable via a simple tweak of the logic which led us to Eq. (5), with the influence from the other "particle" being multiplied by $n/2$ while the background contribution is unchanged:

$$\frac{\mathrm{d}U_{tot}}{\mathrm{d}x}\bigg|_{x^*} = 0 = \frac{2x^*}{w^2} - \left(\frac{n}{2}\right)\frac{4k^2 x^*}{(k-1)s^2}\left(1 - 4\frac{x^{*2}}{s^2}\right)e^{-\frac{4kx^{*2}}{s^2}}$$

$$\implies x^* = 0 \quad \text{or}$$

$$w^2 = \frac{s^2(k-1)}{nk^2}\frac{1}{1 - 4\frac{x^{*2}}{s^2}}e^{\frac{4kx^{*2}}{s^2}}$$

$$w^2 = w_0^2 \frac{e^{\frac{4kx^{*2}}{s^2}}}{1 - 4\frac{x^{*2}}{s^2}} \tag{13}$$

The solution can be written explicitly in terms of the Lambert W function (as done above for the special case $n = 2$), now using w_0 to further simplify:

$$x^*(w) = \frac{s}{2}\sqrt{1 - \frac{1}{k}W\left(ke^k\frac{w_0^2}{w^2}\right)} \tag{14}$$

For $|x| \ll 1$, this is approximately

$$x^* \approx \frac{s}{\sqrt{2w_0(k+1)}}\sqrt{w - w_0}\,.$$

exactly as we saw before (all scaling is accounted for by w_0).

D. Return of stability at the origin

We seek an understanding of the second "major" bifurcation: the birth of the three-stack state near $w = 2w_0$, with a small central stack between the two large symmetric stacks. We can easily check the curvature of the potential landscape at the origin between two equal stacks, using this as a test to identify when a particle would stably rest there. We note that this spot sees an identical contribution from all particles at $\pm x^*$:

$$\frac{\mathrm{d}^2 U_{tot}}{\mathrm{d}x^2}\bigg|_{x=0} = \frac{2}{w^2} + n\left[-\frac{2k^2}{(k-1)s^2}\cdot\right.$$

$$\left.\left(1 - \frac{2k+3}{s^2}x^{*2} + \frac{2k}{s^4}x^{*4}\right)e^{-\frac{kx^{*2}}{s^2}}\right]$$

$$= \frac{2}{w^2} - \frac{2}{w_0^2}\left(1 - \frac{2k+3}{s^2}x^{*2} + \frac{2k}{s^4}x^{*4}\right)e^{-\frac{kx^{*2}}{s^2}}\;;,$$

so the birth of stability happens when this curvature crosses 0, at

$$w_c^2 = w_0^2 \frac{e^{\frac{kx^{*2}}{s^2}}}{1 - \frac{2k+3}{s^2}x^{*2} + \frac{2k}{s^4}x^{*4}}\,. \tag{15}$$

When we combine this condition with the two-stack equilibrium relation for w^2, Eq. (13), we get

$$w_0^2 \frac{e^{\frac{kx_c^{*2}}{s^2}}}{1 - \frac{2k+3}{s^2}x_c^{*2} + \frac{2k}{s^4}x_c^{*4}} = w_0^2 \frac{e^{\frac{4kx_c^{*2}}{s^2}}}{1 - 4\frac{x_c^{*2}}{s^2}}\,,$$

$$1 - 4\frac{x_c^{*2}}{s^2} = \left(1 - \frac{2k+3}{s^2}x_c^{*2} + \frac{2k}{s^4}x_c^{*4}\right)e^{\frac{3kx_c^{*2}}{s^2}}\,,$$

(16)

which defies closed-form solution but which we may numerically approximate for our default parameters $k = 2$ and $s = 1$, yielding $x_c^* \approx 0.324$. We can see that this agrees empirically with the stack width coincident with the birth of stability in our large-n figures like Figs. 4 and 12.

This approximation for x^* in turn allows us to approximate w_c, by using either relation again. Using Eq. (13) with $k = 2, s = 1$, we have

$$w_c^2 = w_0^2 \frac{e^{8x_c^{*2}}}{1 - 4x_c^{*2}}\,,$$

$$x_c^* \approx 0.324176\ldots$$

$$\implies w_c \approx 1.99978w_0\,.$$

This is suspiciously close to $2w_0$, but these approximations were done using 16-digit precision, so it appears to indeed be distinct. We note that this value depends on k (though s may be scaled out as always); for example, for $k = 100$ we have $w_{c,100} \approx 1.791w_0$.

After the central stack's creation, the exchange of particles between central and outer stacks is complicated, since the fraction of the population at the origin influences the position of the outer stacks, which in turn influences the stable fraction at the origin. We observe empirically that the outer stacks drift apart in a roughly linear manner, which may be helpful, though we leave this exploration for future work.

We note that the increasing-w sweep only sees particles at the center when they are kicked out of the outer stacks to populate it. On the decreasing-w pass, however, the center hosts a larger stable population at each w value reached, since continuation from the right causes the accumulation of all nearby particles at the center, where they stay until they are ejected to the outer stacks. It is perhaps counterintuitive that these particles "climb" the global potential as it narrows, but it is nevertheless true; the narrowing background potential pushes the outer stacks inward enough that the center becomes less stable, at which point it is "overstuffed" and repels some of its former constituents to join the other stacks.

The decreasing pass thus acts as a lower bound for the *maximal* stable fraction at the center, and the increasing pass acts as an upper bound on the *minimal* stable fractionation. We expect a continuous band of stable fractionations between those values, as indicated by Fig. 14. We leave further exploration of the bands of stability in the $n \to \infty$ limit for future work.
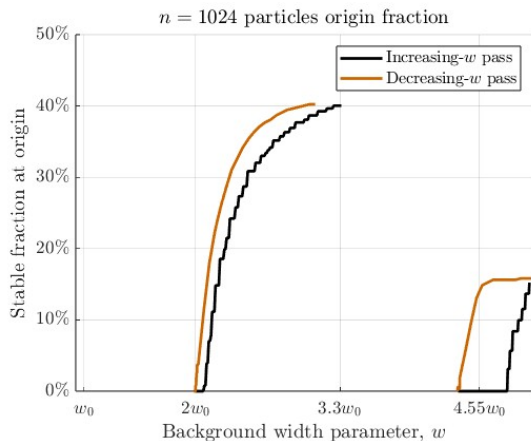
FIG. 14: **Origin fractionation bands,** $n = 1024$. Fraction of population at origin for forward and backward passes with small noise. These curves demonstrate the existence of bands of stability, and are an approximation of those bands. The true bands may be slightly wider, but the fractionations between these curves are stable for corresponding w values.

E. k dependence

The parameter k distorts the equilibrium diagram; in particular, Fig. 15 shows what happens when k grows. We see that large k coincides with a narrower population (smaller range on vertical axis); this is perhaps unintuitive since large k makes the Ricker wavelet's trough shallower, which intuitively means "less stability" overall, and perhaps the dominance of repulsion. However, that would imply a wider population, while in reality we see a narrower one. We might instead take away the competing explanation that the Ricker wavelets' weaker attraction to their preferred distance means the particles don't "buoy" their partners away from the origin as strongly, which leads to more dominance of the background potential-well containment overall.

Asymptotic analysis of Eqs.15 and 16 with large k yields

$$x_c \sim \frac{\alpha}{\sqrt{k}}, \text{ where}$$
$$(1 - 2\alpha)e^{3\alpha} = 1$$
$$\implies \alpha = \frac{1}{3}W\left(-\frac{3}{2}e^{-3/2}\right) + \frac{1}{2}$$
$$\approx 0.2914, \text{ and}$$
$$w_c \to w_0 e^{2\alpha} \approx 1.791w_0.$$

which seems compatible with the large-k diagrams shown in

Fig. 15.

V. METHODS/SIMULATION DETAILS

Particles were started with random Gaussian positions with standard deviation 0.1 on the small-w end. The positions were updated using ODE45 numerical integration for an initial duration of $T = 20n^{-1/2}$ time units (chosen empirically to approximate equilibration-time scaling with n). Runs at each w value exponentially scaled integration time until all particles had moved less than 0.001 units, or a run ended with $T > 5000n^{-1/2}$ (which occured after 8 doublings, for a maximum total run-time of $10,220n^{-1/2}$ time units for any single w value). This was necessary since equilibration time grows dramatically near bifurcation points.

After each integration converged or hit the time limit at one w value, final positions were recorded and a small random perturbation of each particle's position (Gaussian with standard deviation 0.001) was applied to that ending state before the parameter value w was updated and the next simulation commenced—this ensured we only recorded stable equilibria. This process proceeded from $w = 0.925w_0$ to $5w_0$ before descending along those same values; the black arrows in each diagram indicates the direction of this continuation.

VI. DISCUSSION/CONCLUSION

We have examined a system of particles with first-order coupling through Ricker wavelet potential functions, and found remarkably rich self-organizing behavior. Intuitive small-n cases transition to archetypal large-n limiting behavior, with non-origin bifurcations becoming compacted into invisibility while other, "major" bifurcations (those regarding stability of the origin) persist and stabilize for large n. Multistability abounds, and persists for large n; overlapping hysteresis in the position of individual particles becomes stability bands for fractions of the population.

There is plenty more to be explored with these particles. We have not systematically examined dependence on the parameter k, which controls trough depth, though we showcase some promising initial findings in section IV E in the appendix below. Also of interest is the oscillator interpretation, with these particles living on a finite periodic domain, for which we likewise present some intriguing initial findings in the appendix. Behavior with other types of confinement, such as a finite "hard-walled" box, is also an open question. Some of these model variants may lend themselves to real-world applications such as those mentioned in the introduction.

We hope this work provides a solid foundation for the exploration of this system and its variants, which offer tantalizing glimpses of order governing a wild dynamical zoo of possible behavior.

[1] J. C. Slater, "A simplification of the hartree-fock method," Physical review **81**, 385 (1951).

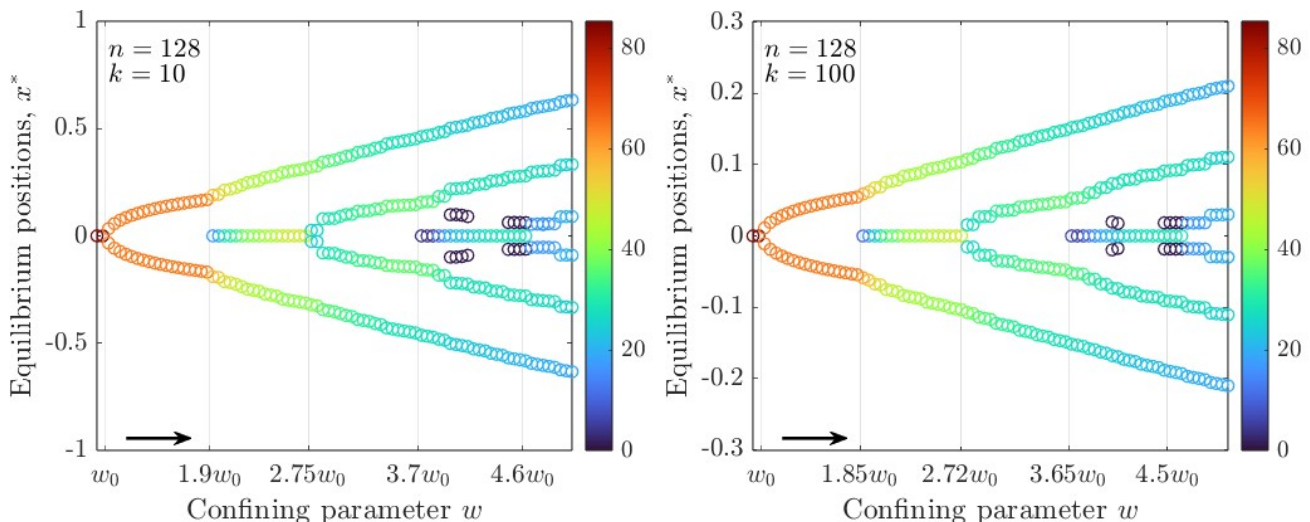[2] Y. Kuramoto, "Self-entrainment of a population of coupled non-

FIG. 15: *k* **dependence.** Equilibrium diagrams for higher values of *k*. The estimated bifurcation values are marked on the *w* axis. As well as narrowing the system in *x*, larger *k* appears to accelerate the bifurcation rate in *w*, but with diminishing returns, hinting at the invariant limit we find in Section IV E: $x_c^* \to\, \approx 0.2914$ and $w_c \to 1.791 w_0$ as $k \to \infty$.

linear oscillators," in *International symposium on mathematical problems in theoretical physics* (Springer, 1975) pp. 420–422.

[3] Z. Csahók, F. Family, and T. Vicsek, "Transport of elastically coupled particles in an asymmetric periodic potential," Physical Review E **55**, 5179 (1997).

[4] P. Schwerdtfeger, N. Gaston, R. P. Krawczyk, R. Tonner, and G. E. Moyano, "Extension of the lennard-jones potential: Theoretical investigations into rare-gas clusters and crystal lattices of he, ne, ar, and kr using many-body interaction expansions," Physical Review B **73**, 064112 (2006).

[5] C. Cohen-Tannoudji, B. Diu, and F. Laloë, *Quantum Mechanics, Volume 3: Fermions, Bosons, Photons, Correlations, and Entanglement* (John Wiley & Sons, 2019).

[6] P. M. M. Maessen, T. A. Rijken, and J. J. de Swart, "Soft-core baryon-baryon one-boson-exchange models. ii. hyperon-nucleon potential," Phys. Rev. C **40**, 2226–2245 (1989).

[7] T. A. Rijken, V. Stoks, and Y. Yamamoto, "Soft-core hyperon-nucleon potentials," Physical Review C **59**, 21 (1999).

[8] G. Yatsenko, E. J. Sambriski, M. A. Nemirovskaya, and M. Guenza, "Analytical soft-core potentials for macromolecular fluids and mixtures," Phys. Rev. Lett. **93**, 257803 (2004).

[9] G. B. Ermentrout and N. Kopell, "Parabolic bursting in an excitable system coupled with a slow oscillation," SIAM journal on applied mathematics **46**, 233–253 (1986).

[10] B. Ermentrout, "Type i membranes, phase resetting curves, and synchrony," Neural computation **8**, 979–1001 (1996).

[11] F. C. Hoppensteadt and E. M. Izhikevich, *Weakly connected neural networks*, Vol. 126 (Springer Science & Business Media, 1997).

[12] There is some multistability with regards to slight asymmetry of these two stacks; for example, sometimes the stacks are 63 and 65 particles, and the system is stable, although in that case their positions are not perfectly symmetric—the larger stack settles slightly closer to the origin.

[13] This notation indicates the partition state of the particles, i.e., the number of particles in each stack, in order. In this case, there are two visibly-distinguishable $1-2$ states since the two-particle stack can be above or below the single-particle stack, though each of those represents six equilibria in full state space

due to permutations of the particles.

Appendix A: Extra Findings

1. Fresh random starts

Without continuation—i.e., when the simulation at each *w* value proceeds from an entirely random starting state rather than a slightly-perturbed version of the previous equilibrium—we see a "fuzzier" but ultimately similar picture; see Fig. 16. This does yield some information about the system's tolerance for asymmetry; the two-stack state for $n = 128$ can be as lopsided as $68 - 60$ in this run and still appear stable. More lopsided stable two-stack states may be possible with biased initial conditions, however.

2. Lennard-Jones and Morse potentials

As mentioned in Section I, the Lennard-Jones and Morse potentials from physics are models of intermolecular potential energy with short-range repulsion and long-range attraction. These potentials may be described in the following forms:

$$U_{\mathrm{LJ}}(x) = 4\varepsilon \left[\left(\frac{x}{\sigma} \right)^{-12} - \left(\frac{x}{\sigma} \right)^{-6} \right],$$

$$U_{\mathrm{M}}(x) = D_e \left[e^{-2a(|x|-r_e)} - 2e^{-a(|x|-r_e)} \right].$$

Fig. 17 shows examples of these potential functions, with as much matching to our default Ricker potential as possible. In particular, this should highlight the limits of their qualitative comparability, and why alteration to a "soft-core" potential amenable to "stacking"/coexistence would be necessary to expect results similar to those presented in this work.
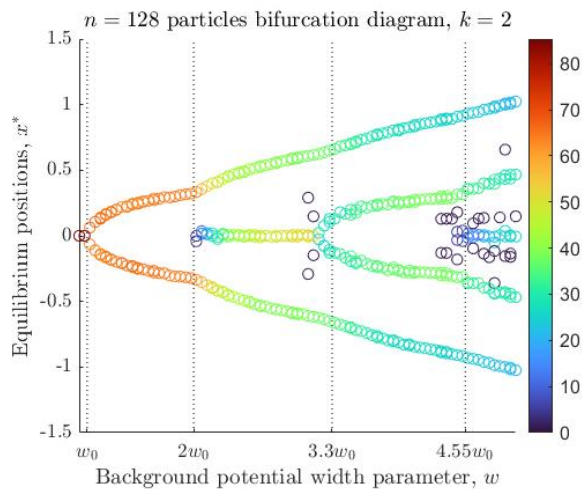
FIG. 16: **Equilibrium diagram without continuation.**
Equilibrium states with a fresh Gaussian random start every
time (and symmetry not enforced). Stack size here gives a
lower bound for tolerance of asymmetric fractionation; the
greatest asymmetry in the two-stack state observed here is
$68 - 60$.
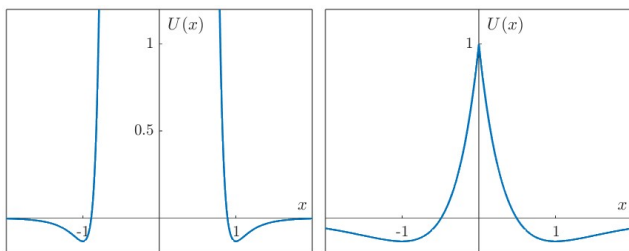
FIG. 17: **Other Classic Potentials.** Examples of the
Lennard-Jones (**left**) and Morse (**right**) potentials from
physics. Parameters have been chosen to match the trough
coordinates of our default-parameter Ricker
potential—$(\pm 1, e^{-2})$—and the peak of $(0, 1)$ for the Morse
potential. Still, we note significant qualitative discrepancies,
namely the infinite central spike for Lennard-Jones and the
"sharp" origin peak for Morse. These qualities preclude the
stability (or even well-defined behavior) of stacking behavior,
and thus the particular richness of behavior we find in our
Ricker system, but alterations to smoothen behavior at the
origin may lead to reconciliation.

3. Ricker Oscillators

A model variant of considerable interest for these Ricker-
potential-coupled particles is their implementation as coupled
oscillators. In this case, their position would represent phase
on a periodic domain, like $(-\pi, \pi]$. A slight tweak to the
Ricker potential would need to be defined to make it periodic;
distance between particles in this space might be taken to be
the shortest distance around the circle, or the infinite sum of
possible distance interpretations at all $\pm 2\pi m$ multiples, or the
potential itself might be made periodic in some other way.
In any case, the parameter s (controlling the location of the
troughs, which acts as a "preferred distance") is no longer re-
movable by scaling in this paradigm; its ratio with the domain
is a qualitatively important value.

Using the simpler, shortest-distance interpretation, we per-
formed simulations and demonstrate the results in Fig. 18. We
found that for small n, the particles did settle uniformly at in-
tervals of s. Sometimes the system took a long time to find
this state, as it evolves more slowly when evenly spaced—
even when the population is more compact than necessary.

However, at large n (such that n times the preferred distance
was much larger than 2π), the system appeared to exhibit
"frozen disorder," or a "glassy" state where particles neither
clump nor uniformly distribute (see Fig. 19). The best lens for
understanding this process appears to be the *cumulative* po-
tential; as the population evolves, it appears to self-organize
almost instantly into a single low frequency wave (created by
many individual Ricker potentials) which then damps quickly
to reveal middle frequencies at smaller amplitude. As the
magnitude of this cumulative potential wave shrinks beneath
the scale of a single wavelet, the inherent higher frequen-
cies of individual particles emerge again (see Fig. 19, bottom
right).

This apparent phenomenon of self-organization in service
of the cumulative potential's frequency-damping is only a nu-
merical observation thus far, and merits future analytical ex-
ploration. It is unclear if this disordered state is truly stable
or merely quasi-stable, and how the parameter-space transi-
tion from even-spacing to disordered "equilibrium" occurs as
the domain becomes overpopulated relative to the preferred
distance. We believe this is a ripe area for future exploration.
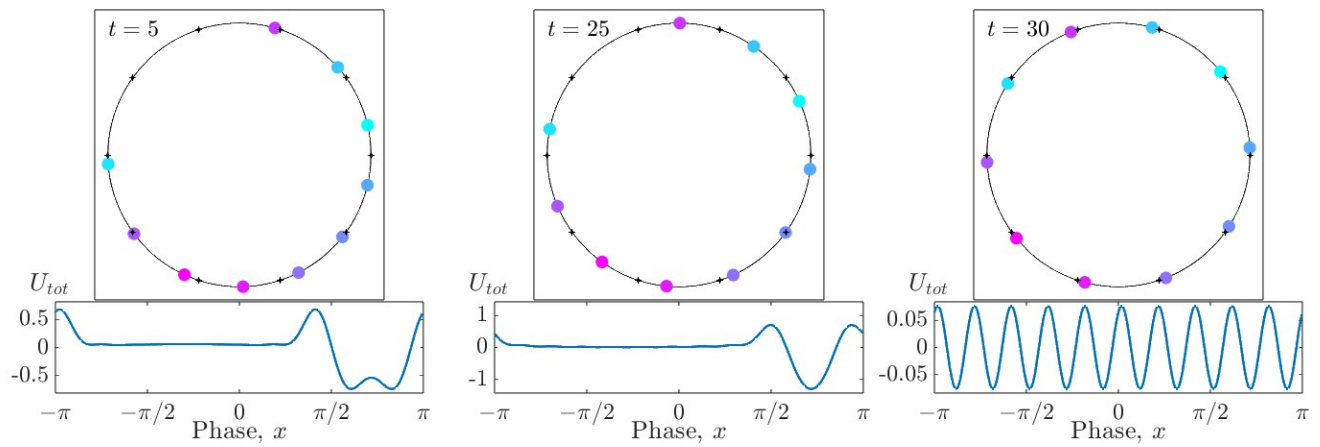
FIG. 18: **Oscillator interpretation, slow convergence.** Ten Ricker oscillators with preferred distance $2\pi/10$. The left figure shows the system at time $t = 5$, central figure at $t = 25$, and right figure at $t = 30$; the population swiftly self-arranges to become near-evenly but too-compactly arranged, then slowly separates, until suddenly "snapping" to perfectly even spacing. Black dots around circle indicate preferred distance; we see the particles eventually space themselves at the same intervals. Color indicates particle index, to distinguish and keep track of them over time.
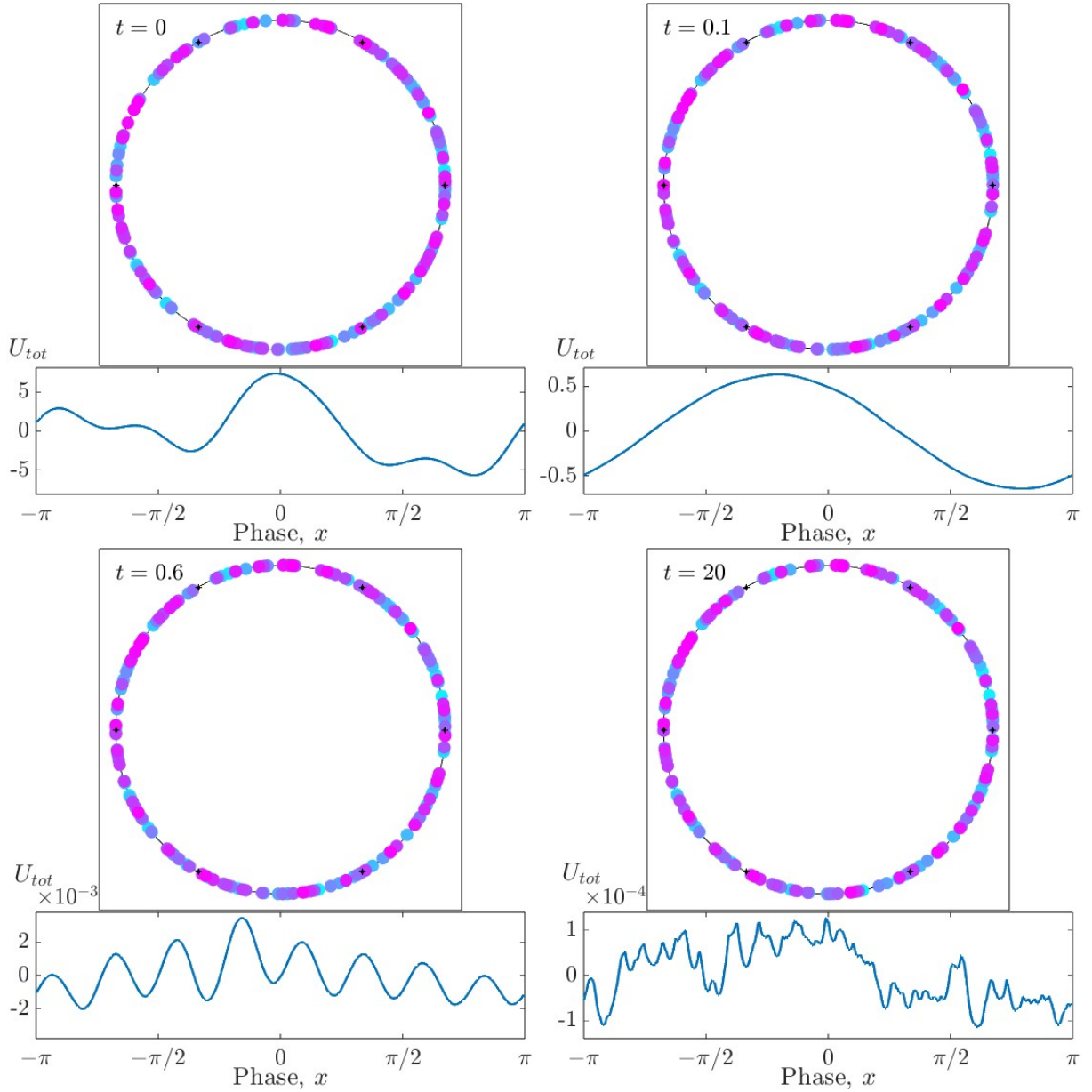
FIG. 19: **Ricker oscillator system.** Two hundred Ricker oscillators with preferred distance $2\pi/6$. **Top left:** Random starting state, and its resulting cumulative potential. **Top right:** At $T = 0.1$, the particles have very quickly arranged themselves into a single low-frequency cumulative-potential wave. **Bottom left:** At $T = 0.6$, the low-frequency wave has damped, leaving a mid-frequency wave (with period $2\pi/8$, higher frequency than the Ricker wavelet's preferred distance) of much lower amplitude (two orders of magnitude smaller), with only minute positional adjustments. **Bottom right:** At $T = 20$, the global potential has damped another order of magnitude, to 1×10^{-4}, leaving only the high-frequency spikes of individual Ricker wavelets (which have a "sharp" nondifferentiable corner as they wrap around $\pm\pi$). This "glassy" and distinctly nonuniform state appears to be stable, though it might only be extremely slow to evolve.